Commun. Comput. Phys.
doi: 10.4208/cicp.191214.071215a

Vol. **19**, No. 4, pp. 881-903
April 2016

Efficient Computation of Nonlinear Crest Distributions for Irregular Stokes Waves

Ying-Guang Wang*

School of Naval Architecture, Ocean and Civil Engineering, Shanghai Jiao Tong University, Shanghai, 200240, China and State Key laboratory of Ocean Engineering, Shanghai Jiao Tong University, Shanghai, 200240, China.

Communicated by Boo-Cheong Khoo

Received 19 December 2014; Accepted (in revised version) 7 December 2015

Abstract. This paper concerns the computation of nonlinear crest distributions for irregular Stokes waves, and a numerical algorithm based on the Fast Fourier Transform (FFT) technique has been developed for carrying out the nonlinear computations. In order to further improve the computational efficiency, a new Transformed Rayleigh procedure is first proposed as another alternative for computing the nonlinear wave crest height distributions, and the corresponding computer code has also been developed. In the proposed Transformed Rayleigh procedure, the transformation model is chosen to be a monotonic exponential function, calibrated such that the first three moments of the transformed model match the moments of the true process. The numerical algorithm based on the FFT technique and the proposed Transformed Rayleigh procedure have been applied for calculating the wave crest distributions of a sea state with a Bretschneider spectrum and a sea state with the surface elevation data measured at the Poseidon platform. It is demonstrated in these two cases that the numerical algorithm based on the FFT technique and the proposed Transformed Rayleigh procedure can offer better predictions than those from using the empirical wave crest distribution models. Meanwhile, it is found that our proposed Transformed Rayleigh procedure can compute nonlinear crest distributions more than 25 times faster than the numerical algorithm based on the FFT technique.

AMS subject classifications: 76B15, 65C50, 65C60, 65C05

Key words: Irregular Stokes waves, crest distribution, Transformed Rayleigh procedure, Fast Fourier Transform (FFT) technique.

1 Introduction

Knowing the wave crest probability distributions is of vital importance to the design and risk analysis of various kinds of ships and marine structures [1, 2]. The probability

*Corresponding author. *Email address:* wyg110@sjtu.edu.cn (Y.-G. Wang)

 ©2016 Global-Science Press

https://doi.org/10.4208/cicp.191214.071215a Published online by Cambridge University Press

distribution of the crest elevation (i.e., the highest elevation of an individual wave) must be established with care because it is used for the calculation of wave loads on a ship or an offshore platform. The extreme wave crest height is a key input parameter for deciding the bow height of a ship in order to avoid green water inundation. Furthermore, a proper statistical knowledge of the extreme wave crest height is essential to define a sufficient air gap under the deck of an offshore platform, and hence to ensure that a wave crest does not endanger the platform's integrity.

It is generally regarded that the wave crest height distributions obey the Rayleigh probability law in an ideal Gaussian random sea [3–7]. In the ideal Gaussian sea model the individual cosine wave trains superimpose linearly (add) without interaction, and therefore, the model is also called the linear sea model. However, waves in the real world are nonlinear [8–10]. Real waves show a small but easily noticed departure from a Gaussian surface. The crests are higher and steeper than expected from a summation of cosine waves with random phase, and the troughs are shallower and smaller [11, 12]. Meanwhile, it should also be pointed out that in the existing literature Lukomsky et al. [13, 14] and Lukomsky and Gandzha [15] have also developed some strongly nonlinear models applicable to extreme wave heights. Consequently, the application of the Rayleigh distribution to the wave crest heights will become invalid, and other more suitable methods should be applied to predict the distribution of wave crests for the nonlinear random model of the sea elevation.

Chakrabarti [1] mentions a model of wave crest height distribution of nonlinear ocean waves. This crest height distribution model was suggested four decades ago by Jahns and Wheeler by performing an empirical correction to the Rayleigh model of the crest height distribution. However, the previous research work of this author's research group has shown that such kind of empirical formulas will sometimes predict wave characteristic distributions that differ considerably from the true ones [16]. In order to overcome the weakness of the empirical approach for predicting the wave crest height distributions, numerical simulations can be performed either through solving the free-surface Euler equations [17, 18] or through Fast Fourier Transforming a wave spectrum. In this article, the author has developed a numerical algorithm based on the Fast Fourier Transform (FFT) technique [19–21] in order to compute the nonlinear crest distributions for irregular Stokes waves. For the numerical implementation of the nonlinear FFT simulation, the problem is divided into two processes, i.e. first generating the first order, linear (Gaussian) time histories with a specific wave spectrum at a specific location, for each of these the numerical algorithm then evaluates the full set of second order corrections. Therefore, the first order wave process, with N components at frequencies ω_n, gives rise to a total of N^2 corrections, spreading over all sum frequencies at frequencies $\omega_n+\omega_m$, and to another N^2 corrections over all difference frequencies $\omega_n-\omega_m$ [22, 23]. However, the nonlinear FFT simulation method as explained above will become very time consuming when N becomes large. Unfortunately, in a typical ocean engineering simulation project, the number N is usually of the order of 1000000 to 40000000. Therefore, there is a great need for a faster approach for computations of crest height distributions.

https://doi.org/10.4208/cicp.191214.071215a Published online by Cambridge University Press

Motivated by the above-mentioned facts, in this paper, in order to further improve the computational efficiency, a new Transformed Rayleigh procedure is also proposed as another alternative for computing the nonlinear wave crest height distributions, and the corresponding computer code has also been developed. Rather than including the second order correction terms to the linear model, the proposed Transformed Rayleigh procedure is to use a deterministic and memoryless functional transformation. The non-Gaussian process of the surface wave elevation is then a continuously differentiable function of a single Gaussian process. Specifically, in our proposed Transformed Rayleigh procedure, the transformation model is chosen to be a monotonic exponential function, calibrated such that the first three moments of the transformed model match the moments of the true process. In this study, the numerical algorithm based on the FFT technique and the proposed Transformed Rayleigh procedure will first be applied for calculating the wave crest height distributions of a sea state with a Bretschneider spectrum corresponding to a water depth of 19.5m, and their computational accuracy will be validated by comparing with the wave crest height distribution results predicted by using the Jahns and Wheeler model and the Theoretical Rayleigh model. Next, the numerical algorithm based on the FFT technique and the proposed Transformed Rayleigh procedure will be applied to predict the wave crest height exceedance probabilities of a sea state with the surface elevation data measured at the Poseidon platform in the Japan Sea, and their computational accuracy will once again be validated.

This paper begins in Section 2 by introducing the knowledge of the irregular Stokes waves. It continues in Section 3 by introducing the numerical algorithm based on the Fast Fourier Transform (FFT) technique for carrying out the computation of the nonlinear crest distributions, and in Section 4 the theoretical background and numerical implementation of the proposed Transformed Rayleigh procedure are elucidated. In Section 5 the calculation examples and discussions will be provided, with conclusions summarized in Section 6.

2 Second order irregular Stokes waves

In the following we briefly introduce the theoretical background of the second order irregular Stokes waves. The fluid region is described using three-dimensional Cartesian coordinates (x,y,z), with x and y the horizontal coordinates, and z the vertical coordinate with the positive z-direction opposing the direction of the gravitational acceleration. Time is denoted by t. The free surface is located at $z=\eta(x,y,t)$. If the fluid is assumed to be ideal, incompressible and inviscid, and the fluid motion irrotational, so that the velocity potential $\Phi(x,y,z,t)$ exists, then for constant water depth d the potential $\Phi(x,y,z,t)$ and the surface elevation $\eta(x,y,t)$ are determined by the following boundary

https://doi.org/10.4208/cicp.191214.071215a Published online by Cambridge University Press

value problem (see, e.g., [24]):

$$\nabla^2\Phi=0, \tag{2.1}$$

$$\frac{\partial\Phi}{\partial t}+\frac{1}{2}(\nabla\Phi)^2+gz=0 \quad \text{at} \quad z=\eta(x,y,t), \tag{2.2}$$

$$\frac{\partial\eta}{\partial t}+\frac{\partial\Phi}{\partial x}\frac{\partial\eta}{\partial x}+\frac{\partial\Phi}{\partial y}\frac{\partial\eta}{\partial y}-\frac{\partial\Phi}{\partial z}=0 \quad \text{at} \quad z=\eta(x,y,t), \tag{2.3}$$

$$\frac{\partial\Phi}{\partial z}=0 \quad \text{at} \quad z=-d. \tag{2.4}$$

Eq. (2.1) is the Laplace equation and Eqs. (2.2), (2.3) and (2.4) are respectively the dynamic free surface boundary condition, the kinematic free surface boundary condition, and the bottom boundary condition. Solutions of the system (2.1)-(2.4) can be sought using the following expansion (see, e.g., [24]):

$$\begin{cases} \Phi=\Phi^{(1)}+\Phi^{(2)}+\cdots \\ \eta=\eta^{(1)}+\eta^{(2)}+\cdots \end{cases} \quad \text{where} \quad \frac{\Phi^{(n+1)}}{\Phi^{(n)}}=\frac{\eta^{(n+1)}}{\eta^{(n)}}=\mathcal{O}(\varepsilon). \tag{2.5}$$

Here ε is a small parameter in the expansion (2.5) and it is typically proportional to the wave steepness. For an irregular sea state characterized by a specific wave power spectral density function (i.e., wave spectrum) $S_{\eta\eta}(\omega)$ where ω is the angular frequency, it is straightforward to show that a first order linear Gaussian solution of the system (2.1)-(2.4) takes the following form (see, e.g., [24]):

$$\Phi^{(1)}(x,t)=\mathrm{Re}\sum_{n=1}^{N}\frac{igc_n}{\omega_n}\frac{\cosh k_n(z+d)}{\cosh k_n d}e^{i(\omega_n t-k_n x+\varepsilon_n)}, \tag{2.6}$$

$$\eta^{(1)}(x,t)=\mathrm{Re}\sum_{n=1}^{N}c_n e^{i(\omega_n t-k_n x+\varepsilon_n)}, \tag{2.7}$$

as N tends to infinity. In Eqs. (2.6) and (2.7), Re denotes the real part of the complex number, and for each elementary sinusoidal wave c_n denotes its complex valued amplitude which is directly related to the specific wave power spectral density function $S_{\eta\eta}(\omega)$. Also in Eqs. (2.6) and (2.7) ω_n is the angular frequency, k_n is the wave number, and ε_n is the phase angle which is assumed to be uniformly distributed in the range of $[0,2\pi]$. Meanwhile, in Eq. (2.7) the individual frequencies, ω_n and wave numbers, k_n are functionally related through the so-called linear dispersion relation:

$$\omega_n{}^2=gk_n\tanh(k_n d) \tag{2.8}$$

where g and d are the acceleration of gravity and water depth, respectively.

Shallow water wave data usually does not follow the linear Gaussian model. The linear Gaussian sea model can be corrected by including quadratic terms. Following

https://doi.org/10.4208/cicp.191214.071215a Published online by Cambridge University Press

Langley [25] and Hasselmann [26] the quadratic corrections are given by:

$$\Phi^{(2)}(x,t)=2\mathrm{Re}\sum_{n=1}^{N}\sum_{m=-1}^{N} ic_nc_mP(\omega_n,\omega_m)\frac{\cosh(k_n+k_m)(z+d)}{\cosh(k_n+k_m)d}e^{i(\omega_nt-k_nx+\varepsilon_n)}e^{i(\omega_mt-k_mx+\varepsilon_n)}$$
$$+2\sum_{n=1}^{N}\frac{{c_n}^2gk_n}{\sinh 2k_nh}t, \tag{2.9}$$

$$\eta^{(2)}(x,t)=\mathrm{Re}\sum_{m=1}^{N}\sum_{n=1}^{N}c_mc_n\left[r_{mn}e^{i(\omega_mt-k_mx+\varepsilon_m+\omega_nt-k_nx+\varepsilon_n)}+q_{mn}e^{i(\omega_mt-k_mx+\varepsilon_m-\omega_nt+k_nx-\varepsilon_n)}\right]. \tag{2.10}$$

In the above two equations, $P(\omega_n,\omega_m)$, r_{mn} and q_{mn} are referred to as quadratic transfer functions. The quadratic transfer function $P(\omega_n,\omega_m)$ is given by:

$$P(\omega_n,\omega_m)=(1-\delta_{-n,m})\frac{\frac{g^2k_nk_m}{2\omega_n\omega_m}-\frac{1}{4}\left({\omega_n}^2+{\omega_m}^2+\omega_n\omega_m\right)+\frac{g^2}{4}\frac{\left(\omega_n{k_m}^2+\omega_m{k_n}^2\right)}{\omega_n\omega_m(\omega_n+\omega_m)}}{(\omega_n+\omega_m)-g\frac{k_n+k_m}{(\omega_n+\omega_m)}\tanh((k_n+k_m)d)}. \tag{2.11}$$

The Kroenecker delta ($\delta_{-n,m}=1$ if $n+m=0$, zero otherwise) is introduced to avoid a singular $P(\omega_n,\omega_m)$.

The quadratic transfer functions r_{mn} and q_{mn} are given by:

$$r_{mn}=-\left(\frac{1}{g}\right)\left(\frac{\left(\frac{1}{4\omega_m\omega_n}\right)2(\omega_m+\omega_n)\left({\omega_n}^2{\omega_m}^2-k_nk_mg^2\right)+\omega_n\left({\omega_m}^4-g^2{k_m}^2\right)+\omega_m\left({\omega_n}^4-g^2{k_n}^2\right)}{(\omega_m+\omega_n)^2\cosh((k_m+k_n)d)-g(k_m+k_n)\sinh((k_m+k_n)d)}\right)$$
$$\times(\omega_m+\omega_n)\cosh((k_m+k_n)d)-\left(\frac{1}{4g\omega_m\omega_n}\right)\left(k_mk_ng^2-{\omega_n}^2{\omega_m}^2\right)+\left(\frac{1}{4g}\right)\left({\omega_m}^2+{\omega_n}^2\right), \tag{2.12}$$

$$q_{mn}=-\left(\frac{1}{g}\right)\left(\frac{\left(\frac{1}{4\omega_m\omega_n}\right)2(\omega_m-\omega_n)\left({\omega_n}^2{\omega_m}^2+k_nk_mg^2\right)-\omega_n\left({\omega_m}^4-g^2{k_m}^2\right)+\omega_m\left({\omega_n}^4-g^2{k_n}^2\right)}{(\omega_n-\omega_m)^2\cosh(|k_m-k_n|d)-g|k_n-k_m|\sinh(|k_n-k_m|d)}\right)$$
$$\times(\omega_n-\omega_m)\cosh(|k_n-k_m|d)-\left(\frac{1}{4g\omega_m\omega_n}\right)\left(k_mk_ng^2+{\omega_n}^2{\omega_m}^2\right)+\left(\frac{1}{4g}\right)\left({\omega_m}^2+{\omega_n}^2\right), \tag{2.13}$$

where the wave numbers k_n and frequencies ω_n in the above equations satisfy the same relation as in the linear model. Finally, by combining Eq. (2.7) and Eq. (2.10) the wave surface elevations for the second order irregular Stokes waves can be written as:

$$\eta(x,t)=\eta^{(1)}(x,t)+\eta^{(2)}(x,t)$$
$$=\mathrm{Re}\sum_{n=1}^{N}c_ne^{i(\omega_nt-k_nx+\varepsilon_n)}$$
$$+\mathrm{Re}\sum_{m=1}^{N}\sum_{n=1}^{N}c_mc_n\left[r_{mn}e^{i(\omega_mt-k_mx+\varepsilon_m+\omega_nt-k_nx+\varepsilon_n)}+q_{mn}e^{i(\omega_mt-k_mx+\varepsilon_m-\omega_nt+k_nx-\varepsilon_n)}\right]. \tag{2.14}$$

https://doi.org/10.4208/cicp.191214.071215a Published online by Cambridge University Press

Here, it is specified that Eqs. (2.9)-(2.13) describing the so-called quadratic transfer functions are a partial case of Zakharov's Hamiltonian equations describing multiple wave interactions (see, e.g. Krasitskii [27]).

3 The numerical algorithm based on the Fast Fourier Transform technique for nonlinear computations

We have obtained Eq. (2.14) for the computation of the wave surface elevations for the second order irregular Stokes waves. For the numerical implementation, we divide this problem into two processes, i.e. first generating a first order linear (Gaussian) wave process with a specific wave power spectral density function (i.e. wave spectrum) $S_{\eta\eta}(\omega)$, then adding to it the nonlinear corrections based on second order hydrodynamics. Input to our numerical algorithm include the first order wave power spectral density function $S_{\eta\eta}(\omega)$, the water depth, and a fixed location at which the wave elevation time histories are to be computed. The obtained time histories can then be statistically processed to obtain the wave crest height distributions.

In implementing our numerical algorithm, the Fast Fourier Transform (FFT) techniques are first utilized to generate the first order, linear (Gaussian) time histories at the specific location (An FFT computes the Discrete Fourier Transform and produces exactly the same result as evaluating the Discrete Fourier Transform definition directly; the most important difference is that an FFT is much faster.). For each of these our numerical algorithm then evaluates the full set of second order corrections according to the hydrodynamic theory as specified in Section 2. Therefore, the first order wave process, with N components at frequencies ω_n, gives rise to a total of N^2 corrections, spreading over all sum frequencies at frequencies $\omega_n+\omega_m$, and to another N^2 corrections over all difference frequencies $\omega_n-\omega_m$. In the following the underlying theories of our numerical algorithm are briefly illustrated.

In this study we consider $\eta^{(1)}$ in Eq. (2.7) at a specific reference location (say $x=0$) and rewrite it as $\eta_G(t)$ to indicate that it is the linear (Gaussian) part of the waves. For a total time period T of computation, Eq. (2.7) can be written as:

$$\eta_G(t)=\mathrm{Re}\sum_{n=1}^{N}c_n e^{i(\omega_n t+\varepsilon_n)}=\sum_{n=1}^{N}c_n\cos(\omega_n t+\varepsilon_n). \tag{3.1}$$

For the computation of the linear, first order Gaussian waves, the desired number of computed points, $npts$, (and thus the total time duration to be computed, T) is requested as inputs. To take advantage of the discrete Fast Fourier Transform techniques, it assumes a regular spacing $\Delta t=T/npts$ between points. Eq. (3.1) can then be rewritten as:

$$\eta_G(t)=\mathrm{Re}\sum_{n=1}^{npts}X_n e^{i\omega_n t}=\sum_{n=1}^{npts/2}c_n\cos(\omega_n t+\varepsilon_n). \tag{3.2}$$

https://doi.org/10.4208/cicp.191214.071215a Published online by Cambridge University Press

Here X_n are complex Fourier coefficients. The lower half of these directly reflect both the random amplitude c_n and phase ε_n at frequency $\omega_n = n \bullet \Delta\omega$:

$$X_n = \frac{1}{2} c_n e^{i\varepsilon_n}, \qquad n = 1, \cdots, npts/2. \tag{3.3}$$

The upper half are in turn taken as the complex conjugates (the symbol "*") of the lower half:

$$X_{npts-n} = X_n *, \qquad n = 1, \cdots, npts/2. \tag{3.4}$$

Here we should mention that we have the relation $\Delta\omega = \omega_c / N$ and ω_c is the upper cut off frequency beyond which the power spectral density function $S_{\eta\eta}(\omega)$ may be assumed to be zero for either mathematical or physical reasons. The value of the upper cut off frequency ω_c can be established using the following formula (Shinozuka and Deodatis [28]):

$$\int_0^{\omega_c} S_{\eta\eta}(\omega) \mathrm{d}\omega = (1-\epsilon) \int_0^{\infty} S_{\eta\eta}(\omega) \mathrm{d}\omega \tag{3.5}$$

with ϵ chosen to be a very small positive number ($0 < \epsilon \ll 1$, e.g. $\epsilon = 0.01$, $\epsilon = 0.001$). At this point it should be noted that when generating sample functions of the computed stochastic process according to Eq. (3.2), the time step Δt separating the generated values of $\eta_G(t)$ in the time domain has to obey the Nyquist frequency condition (Shinozuka and Deodatis [28]):

$$\Delta t \leqslant 2\pi / (2\omega_c). \tag{3.6}$$

The above condition is necessary in order to avoid aliasing according to the sampling theorem (Shinozuka and Deodatis [28]).

Eqs. (3.3)-(3.4) reflect that unique information is contained only in the lower half frequencies; indeed, any information in the upper half frequencies (above the Nyquist) is obscured by aliasing.

Thus, the first order wave process is generated by assigning random c_n and ε_n defining X_n from Eqs. (3.3)-(3.4), and finally take the inverse Fourier Transform to recover the discretized time history $\eta_G(t_j)$. To see this, note that since $\Delta t \bullet \Delta\omega = 2\pi / npts$, Eq. (3.2) can be evaluated at $t = t_j$ to give that:

$$\eta_G(t_j) = \mathrm{Re} \sum_{n=1}^{npts} X_n e^{2\pi i j n / npts}. \tag{3.7}$$

This is precisely the definition of the discrete Fast Fourier Transform (FFT). We show as an example to use Eq. (3.7) to calculate the linear Gaussian wave time histories of a sea state with a standard Bretschneider spectrum corresponding to a water depth of 19.5m. The mathematical expression of the Bretschneider frequency spectrum with a significant wave height Hs and spectral peak frequency ω_p is as follows [5]:

$$S_{\eta\eta}(\omega) = \frac{1.25}{4} \frac{(\omega_p)^4}{\omega^5} {H_S}^2 \exp\left(-\frac{5}{4} \left(\frac{\omega_p}{\omega} \right)^4 \right) \tag{3.8}$$

https://doi.org/10.4208/cicp.191214.071215a Published online by Cambridge University Press

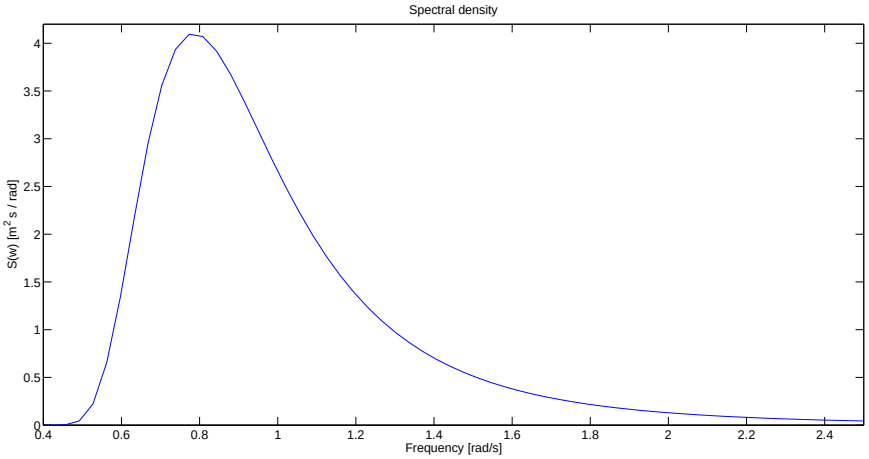


Figure 1: Bretschneider spectrum with $Hs=6$m and $T_p=8.0$s.

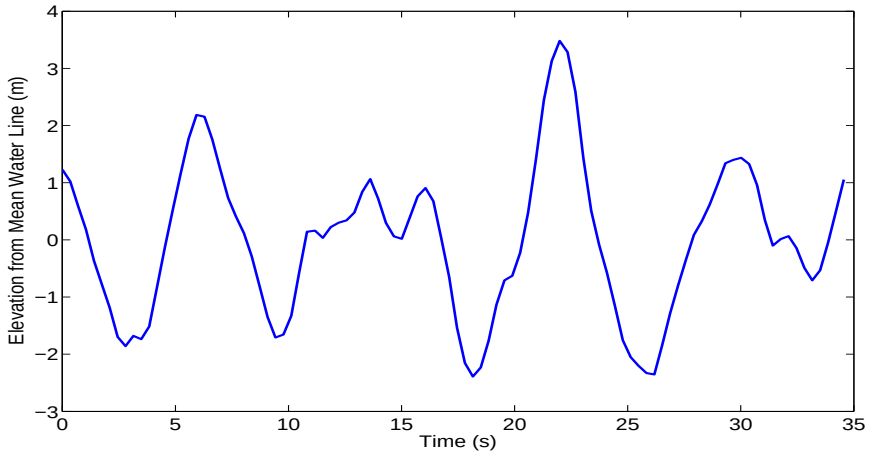


Figure 2: FFT computation of the linear part $\eta_G(t)$ which contains 100 wave elevation points.

where $\omega_p=2\pi/T_p$ and T_p is the spectral peak period. In our calculation example, the significant wave height is taken to be $Hs=6$m and the spectral peak period is taken to be $T_p=8.0$s. Fig. 1 shows the chosen Bretschneider spectrum with $Hs=6$m and $T_p=8.0$s.

Fig. 2 shows the FFT computation of the linear part wave elevation time series $\eta_G(t)$ which contains 100 wave elevation points. A wave elevation point has two coordinates (The first coordinate is time. The second coordinate is the value of the wave elevation above the mean water level.). The computation is based on Eq. (3.7) and the Bretschneider spectrum as shown in Fig. 1.

Next we consider the nonlinear correction $\eta^{(2)}$ in Eq. (2.10) at a specific reference

https://doi.org/10.4208/cicp.191214.071215a Published online by Cambridge University Press

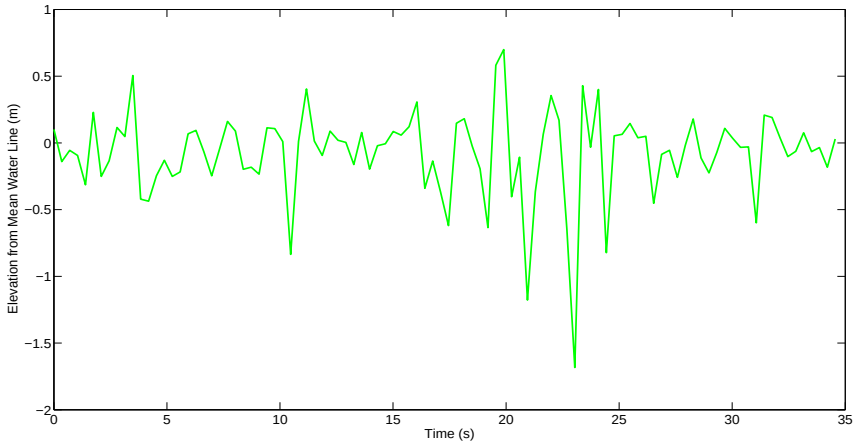


Figure 3: FFT computation of the nonlinear part $\eta_{SO}(t)$ which contains 100 wave elevation points.

location (say $x=0$) and rewrite it as $\eta_{SO}(t)$ to indicate that it is the second order correction part of the waves. The second order correction is generated similarly as the first order one, starting with Eq. (2.10), substituting $N=npts/2$ in Eq. (3.2) and X_n from Eq. (3.3):

$$\eta_{SO}(t)=4\mathrm{Re}\sum_{m=1}^{npts/2}\sum_{n=1}^{npts/2}\left[X_mX_nr_{mn}e^{i(\omega_m+\omega_n)t}+X_mX_n*q_{mn}e^{i(\omega_m-\omega_n)t}\right]. \tag{3.9}$$

The leading factor reflects a net factor of 4 because c_mc_n is $4X_mX_n$, the program then seeks to rewrite both the sum frequency and difference frequency contributions in a Fourier sum analogous to Eq. (3.7). For example, the sum frequency is assumed to be of the form:

$$\eta_{SO}{}^{+}(t_j)=\mathrm{Re}\sum_{k=1}^{npts}Y_ke^{2\pi ijn/npts}. \tag{3.10}$$

The output Fourier coefficients, Y_k, are evaluated by equating Eqs. (3.9) and (3.10). This implies a sum over all wave frequency pairs (ω_m,ω_n) in Eq. (3.9) that gives rise to sum frequency ω_k. The difference frequency Fourier coefficients are constructed in a similar way, and added on the sum frequency Y_k coefficients. Once these combined Y_k coefficients are found a (one dimensional) inverse Fast Fourier Transform is performed to recover the second order time history. Fig. 3 shows the FFT computation of the second order part wave elevation time series $\eta_{SO}(t)$ which contains 100 wave elevation points. The computation is also based on the Bretschneider spectrum with $Hs=6$m and $T_p=8.0$s as shown in Fig. 1.

Finally, the entire irregular Stokes waves $\eta(t)$ can be obtained by combing the linear part $\eta_G(t)$ and the second order part $\eta_{SO}(t)$, i.e.:

$$\eta(t)=\eta_G(t)+\eta_{SO}(t). \tag{3.11}$$

https://doi.org/10.4208/cicp.191214.071215a Published online by Cambridge University Press

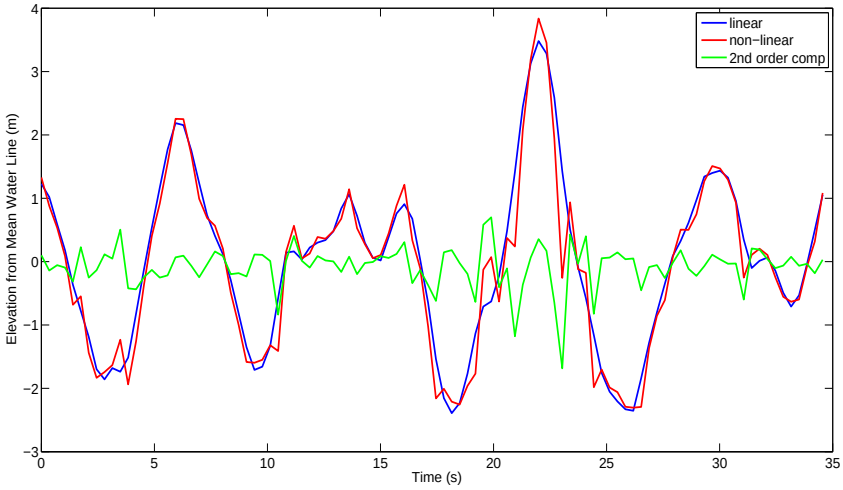


Figure 4: FFT computation of the red curve non-linear wave $\eta(t)$, the blue curve linear wave $\eta_G(t)$ and the green curve 2nd order correction wave $\eta_{SO}(t)$ respectively of 100 points wave elevation time series.

In Fig. 4 the red curve shows the FFT computation of the entire $\eta(t)$ (the linear part $\eta_G(t)$ plus the second order part $\eta_{SO}(t)$) wave elevation time series which contains 100 wave elevation points. The computation is also based on the Bretschneider spectrum with $Hs=6$m and $T_p=8.0$s as shown in Fig. 1. In Fig. 4, the blue curve shows the FFT computation of the linear part wave elevation time series $\eta_G(t)$ which contains 100 wave elevation points. In Fig. 4. the green curve shows the FFT computation of the second order correction part wave elevation time series $\eta_{SO}(t)$ which also contains 100 wave elevation points. We can see that the wave crests have become steeper and higher.

Based on the above FFT computed entire wave elevation time series $\eta(t)$, the wave crest height time series can subsequently be extracted. After extracting these crest height time series, exact Epanechnikov kernel density estimates can then be carried out for obtaining the probability density function of the wave crest heights. Next, cumulative trapezoidal numerical integration can be performed on the above-mentioned probability density function for getting the probability distribution (F) of the wave crest heights. Finally, the wave crest height exceedance probabilities can be obtained based on the probability distribution by utilizing the formula $P=1-F$. These above-mentioned calculation procedures will be used in two specific calculation examples in Section 5 and the FFT computed wave crest height exceedance probabilities will be shown there.

However, the above FFT process is still somewhat time consuming, therefore in this paper we also propose a Transformed Rayleigh procedure to further improve the computational efficiency. In the next section, the theoretical background of the proposed Transformed Rayleigh procedure will be elucidated.

https://doi.org/10.4208/cicp.191214.071215a Published online by Cambridge University Press

4 The proposed Transformed Rayleigh procedure

As shown in Appendix A, the entire irregular Stokes waves $\eta(t)$ can be expressed as (which is also sometimes referred to as Kac-Siegert's solution):

$$\eta(t)=\sum_{j=1}^{2N}\beta_j Z_j+\lambda_j {Z_j}^2 \tag{4.1}$$

where Z_j are independent Gaussian processes with unit variance, and β_j and λ_j are coefficients computed based on the information provided by the sea spectrum $S_{\eta\eta}(\omega)$, which is chosen for a given sea state.

From Section 3 we know that $\eta(t)$ is the height of the sea level at a fixed point as a function of time t. We here use the so called mean down crossing wave to define a wave, i.e. the wave is considered as a part of a function between the consecutive down crossings of the mean sea level. Assume $\eta(t)$ crosses a mean sea level u, finite many times and denote the times of down crossings of u_* by t_i, $0<t_1<t_2<\cdots,$. The crest M_j^*, say, of the ith wave is the global maximum of $\eta(t)$ during the interval $t_i<t<t_{i+1}$.

The goal of the Transformed Rayleigh procedure is, as the name suggests, to model the sea surface elevation as a non-Gaussian process but using the knowledge associated with the Gaussian processes. This is achieved through a transformation function $G(\cdot)$. More precisely, we shall model the sea surface elevation by a process $\eta(t)$ which is a function of a single stationary Gaussian process $\tilde{\eta}(t)$ with mean value $\tilde{\mu}$ and variance $\tilde{\sigma}^2$, i.e. we can re-express Eq. (4.1) as:

$$\eta(t)=G(\tilde{\eta}(t))=\tilde{\eta}(t)+\zeta^*(\tilde{\eta}(t))^2 \qquad \frac{dG}{d\eta}>0, \qquad G(0)=0. \tag{4.2}$$

Note that once the distributions of crests in $\tilde{\eta}(t)$ are computed, then the corresponding wave crest distributions in $\eta(t)$ are obtained by simple transformations involving only the inverse of G, which we shall denote by g^* here. Actually we shall use the function g^* to define the transformation instead of G, and use the relation $\tilde{\eta}(t)=g^*(\eta(t))$ between the real sea data $\eta(t)$ and the transformed data $\tilde{\eta}(t)$. In our research, the transformation model is chosen to be a monotonic exponential function, calibrated such that the first three moments of the transformed model $G(\tilde{\eta}(t))$ match the moments of the true process $\eta(t)$. Information about the moments of the process can be obtained by resorting to theoretical models (see Appendix B). Therefore, the functional relationship between $\eta(t)$ and $\tilde{\eta}(t)$ given in Eq. (4.2) is inversely presented such that the random process $\tilde{\eta}(t)$ is expressed approximately as a function of $\eta(t)$ as follows [5]:

$$\tilde{\eta}(t)=\frac{1}{\gamma\zeta}(1-\exp(-\gamma\zeta\eta(t))) \tag{4.3}$$

where γ is a constant: 1.28 for $\eta(t)\geq 0$, and 3.0 otherwise. In order to determine the

https://doi.org/10.4208/cicp.191214.071215a Published online by Cambridge University Press

unknown parameters ζ, $\tilde{\mu}$ and $\tilde{\sigma}^2$ in the above equation, we first write Eq. (4.2) as follows:

$$\eta(t)=\left[\sqrt{\zeta}\left(\tilde{\eta}(t)+\frac{1}{2\zeta}\right)\right]^2-\frac{1}{4\zeta}. \tag{4.4}$$

The characteristic function of $\eta(t)$ can be obtained as follows [5]:

$$\phi(t)=\frac{1}{1-2\zeta\tilde{\sigma}^2t}\exp\left[\left(\zeta\tilde{\mu}^2+\tilde{\mu}+\frac{\tilde{\sigma}^2}{2}it\right)\left(\frac{it}{1-2i\zeta\tilde{\sigma}^2t}\right)\right]. \tag{4.5}$$

By taking the logarithm of the characteristic function and expanding it in a series of (it), we obtain the following cumulant generating function [29]:

$$\begin{aligned}\psi(t)=\ln\phi(t)=&\left(\zeta\tilde{\sigma}^2+\zeta\tilde{\mu}^2+\tilde{\mu}\right)(it)+\left(\zeta^2\tilde{\sigma}^4+\frac{\tilde{\sigma}^2}{2}+2\zeta\tilde{\sigma}^2\left(\zeta\tilde{\mu}^2+\tilde{\mu}\right)\right)(it)^2\\&+\left(\frac{4}{3}\zeta^3\tilde{\sigma}^6+\zeta\tilde{\sigma}^4+4\zeta^2\tilde{\sigma}^4\left(\zeta\tilde{\mu}^2+\tilde{\mu}\right)\right)(it)^3+\cdots.\end{aligned} \tag{4.6}$$

Similarly, by taking the logarithm of the characteristic function of the Kac-Siegert solution in Eq. (4.1) and expanding it in a series of (it), we obtain the following cumulant generating function [5]:

$$\begin{aligned}\psi(t)=\ln\phi(t)=&\frac{-1}{2}\sum_{j=1}^{2N}\ln\left(1-2i\lambda_jt\right)-\sum_{j=1}^{2N}\frac{\beta_jt^2}{2}\frac{1}{1-2i\lambda_jt}\\=&\left(\sum_{j=1}^{2N}\lambda_j\right)it+\frac{1}{2!}\left(\sum_{j=1}^{2N}{\beta_j}^2+2\sum_{j=1}^{2N}{\lambda_j}^2\right)(it)^2+\frac{1}{3!}\left(6\sum_{j=1}^{2N}\lambda_j{\beta_j}^2+8\sum_{j=1}^{2N}{\lambda_j}^3\right)(it)^3+\cdots.\end{aligned} \tag{4.7}$$

In the above equation we have the relation $\sum_{j=1}^{2N}\lambda_j=0$ because the mean value of $\eta(t)$ is zero. By comparing Eq. (4.6) and Eq. (4.7) we obtain the following relationships:

$$\begin{aligned}&\zeta\tilde{\sigma}^2+\zeta\tilde{\mu}^2+\tilde{\mu}=0,\\&\tilde{\sigma}^2-2\zeta^2\tilde{\sigma}^4=\sum_{j=1}^{2N}{\beta_j}^2+2\left(\sum_{j=1}^{2N}{\lambda_j}^2\right),\\&3\zeta\tilde{\sigma}^4-8\zeta^3\tilde{\sigma}^6=3\left(\sum_{j=1}^{2N}\lambda_j{\beta_j}^2\right)+4\left(\sum_{j=1}^{2N}{\lambda_j}^3\right).\end{aligned} \tag{4.8}$$

Because β_j and λ_j in the above three sets of equations can be computed based on the information provided by the sea spectrum $S_{\eta\eta}(\omega)$ which is chosen for a given sea state, the unknown parameters ζ, $\tilde{\mu}$ and $\tilde{\sigma}^2$ can be readily obtained by solving the above three sets of algebra equations. Then we can obtain the functional transformation g^* (i.e. the inverse of $G: G^{-1}$). Next, we turn to the calculation of the probability distribution $F_{M^*}(h)$

https://doi.org/10.4208/cicp.191214.071215a Published online by Cambridge University Press

of the nonlinear crest h for the irregular Stokes waves. As shown in Wang and Xia [30], we have that:

$$F_{M^*}(h)=1-\exp\left(-\frac{\left(G^{-1}(h)\right)^2}{2}\right). \tag{4.9}$$

We notice that the exponent in the right part of equation (4.9) is the Rayleigh probability that the linear crest exceeds the predefined threshold h. That is why this model is called a Transformed Rayleigh procedure.

Summarizing the above derivation process (including the derivation process in Appendix A) we can find that the advantages of utilizing our proposed Transformed Rayleigh procedure for calculating the wave crest height distributions are as follows: The computational burden will be reduced to calculating the eigenvalues and eigenvectors of two matrices and subsequently solving three sets of algebra equations. The elements in these two matrices are directly related to the wave spectrum and the quadratic transfer functions r_{mn} and q_{mn}. The above mentioned calculation procedures can be conveniently and efficiently executed by using some standard routines in MATLAB (matrix laboratory), which is a fourth generation numerical computing environment. Finally, the solutions of the three sets of algebra equations can be inserted in an exponential function and the transformed Rayleigh distribution can be readily obtained.

5 The computation examples and discussions

In this section we utilize our numerical algorithm based on the Fast Fourier Transform technique and our proposed Transformed Rayleigh procedure to respectively compute the nonlinear crest height distributions of irregular Stokes waves based on a standard spectrum and measured data at the Poseidon platform. Poseidon platform was located 3 km off the coast of Yura in the Yamagata prefecture, in the Japan Sea during the measurements [31]. Fig. 5 shows the geographical position of the coast of Yura.

Fig. 6 shows our calculation results of the wave crest height exceedance probabilities for a sea state with a Bretschneider spectrum with $Hs=6.0$m and $T_p=8.0$s for a water depth of 19.5m.

The solid green line in Fig. 6 represents the Fast Fourier Transform nonlinear computation results of the wave crest height exceedance probability of this irregular sea state. In this Fast Fourier Transform nonlinear computation, 3500000 wave elevation points (350 repetitions of a computation of 10000 wave elevation points) are generated in the computed time series in order to reduce the variance of the calculation. The above Fast Fourier Transform nonlinear computation is based on the Eqs. (3.1)-(3.11) as specified in Section 3 while the random phase angles is designated to be uniformly distributed in the range of $[0,2\pi]$. During the computation, the sampling interval is defined by the Nyquist frequency (i.e. by using Eq. (3.6) in Section 3). The wave crest height time series are subsequently extracted from these 3500000 wave elevation points. After extracting these crest height time series, exact Epanechnikov kernel density estimates are carried out for

https://doi.org/10.4208/cicp.191214.071215a Published online by Cambridge University Press

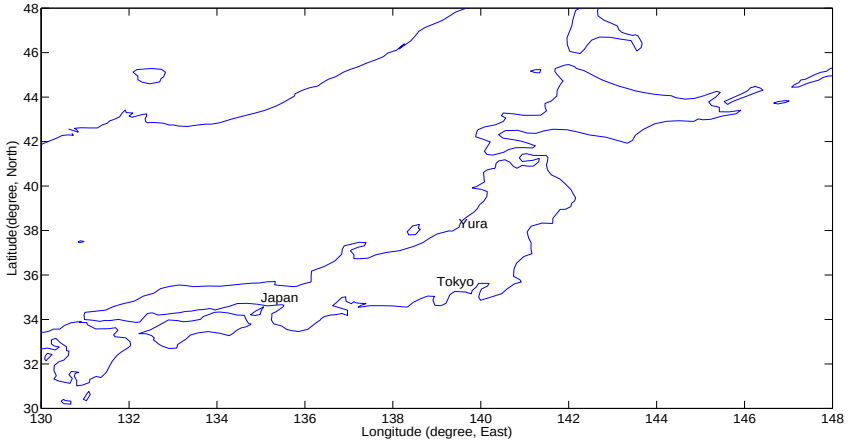


Figure 5: The geographical position of the coast of Yura.

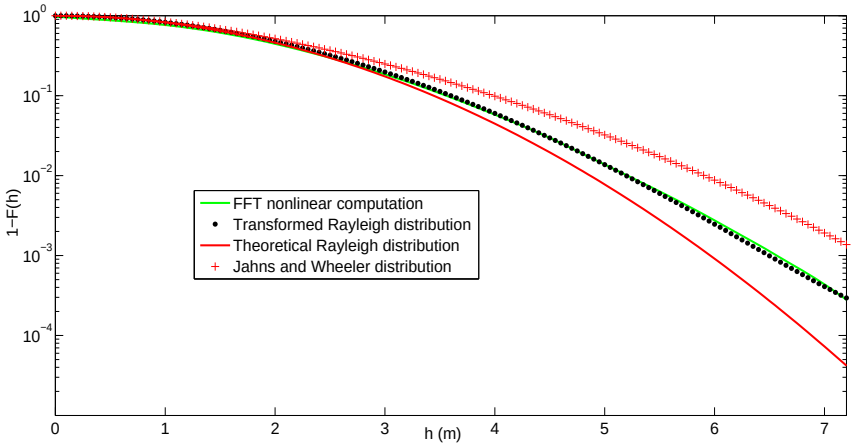


Figure 6: Wave crest height exceedance probabilities for a sea state with a Bretschneider spectrum with $Hs=6.0$m and $T_p=8.0$s for a water depth of 19.5m.

obtaining the probability density function of the wave crest heights. Here we should mention that some kinds of kernel density functions are commonly used: uniform, biweight, triweight, triangle, tricube, Epanechnikov, Gaussian, and cosine. However, the kernel density function that minimizes the mean integrated square error is the Epanechnikov kernel, which has the following expression:

$$K(h)=\frac{3}{4}\left(1-h^2\right)\mathbf{1}_{\{|h|\leqslant 1\}} \tag{5.1}$$

where $\mathbf{1}_{\{|h|\leqslant 1\}}$ is the indicator function. The Epanechnikov kernel density function is used

https://doi.org/10.4208/cicp.191214.071215a Published online by Cambridge University Press

in this article to obtain the probability density function of the wave crest heights based on which the wave crest height exceedance probabilities can finally be obtained. The above Fast Fourier Transform nonlinear computation results can be used as the benchmark against which the accuracy of the results from the proposed Transformed Rayleigh procedure or from the empirical crest distribution models is checked.

In Fig. 6, the solid black dots represent the results of the wave crest height exceedance probabilities obtained from utilizing our proposed Transformed Rayleigh procedure. In applying the Transformed Rayleigh procedure, two 257×257 matrices $[Q+R]$ and $[Q-R]$ as specified in Eq. (A.14) are first calculated and the elements in these two matrices are directly related to the Bretschneider wave spectrum as shown in Fig. 1 and the quadratic transfer functions r_{mn} and q_{mn}. Then the standard MATLAB routine "eig" is utilized to perform the eigenvalue decomposition on the two matrices $[Q+R]$ and $[Q-R]$ so that the two matrices P_1 and P_2 as specified in in Eq. (A.15) can be obtained. Next, the standard MATLAB routine "diag" is utilized to obtain the two matrices Λ_1 and Λ_2 as specified in Eq. (3.1). Subsequently the coefficients β_j and λ_j are calculated by using Eq. (A.18) based on the Bretschneider wave spectrum in Fig. 1, and the mean value $\tilde{\mu}$ and variance $\tilde{\sigma}^2$ of the stationary Gaussian process $\tilde{\eta}(t)$ are obtained by solving the three sets of algebra equations in Eq. (4.8). Finally, the G^{-1} function is calculated by using Eq. (4.3) in Section 4 and the Transformed Rayleigh distribution is calculated by using Eq. (4.9). We can see that the results from the Transformed Rayleigh procedure fit the Fast Fourier Transform nonlinear computation results very well.

In Fig. 6, the solid red line represents the wave crest height exceedance probabilities calculated by using the Theoretical Rayleigh model which is based on the linear wave theory. We notice that the Theoretical Rayleigh method underestimates the exceedance probabilities in the wave crest height region of about [3m, 7.2m]. In Fig. 6, the small red "+" represents a wave crest height exceedance probability predicted by using the following Jahns and Wheeler wave crest height distribution model [1]:

$$F(A_c<h)=1-\exp\left\{-8\left(\frac{h}{H_s}\right)^2\left[1-\beta_1\frac{h}{d}\left(\beta_2-\frac{h}{d}\right)\right]\right\},\qquad h\geqslant 0, \tag{5.2}$$

where h is the crest height, H_S is the significant wave height, β_1 and β_2 are empirical coefficients. $\beta_1=4.37$ and $\beta_2=0.57$ are recommended in [1]. We can find that the Jahns and Wheeler wave crest height distribution model gives poorer predictions in the wave crest height region of about [2m, 7.2m] than the Transformed Rayleigh distribution does.

Finally, it is mentioned that in this case, the time series computation with 3500000 wave elevation points and the post statistical processing for getting the green curve in Fig.6 take about 86 seconds on a desktop computer (HP dx2310MT (VP784PA), Pentium (R) Dual-Core CPU E5300@2.60GHz). By comparison, it takes less than 3 seconds to obtain the results of the wave crest height exceedance probabilities represented by the black solid dots in Fig. 6 by applying the Transformed Rayleigh procedure. The accuracy and efficiency of the Transformed Rayleigh procedure for calculating the wave crest height distributions of irregular Stokes waves can thus be validated.

https://doi.org/10.4208/cicp.191214.071215a Published online by Cambridge University Press

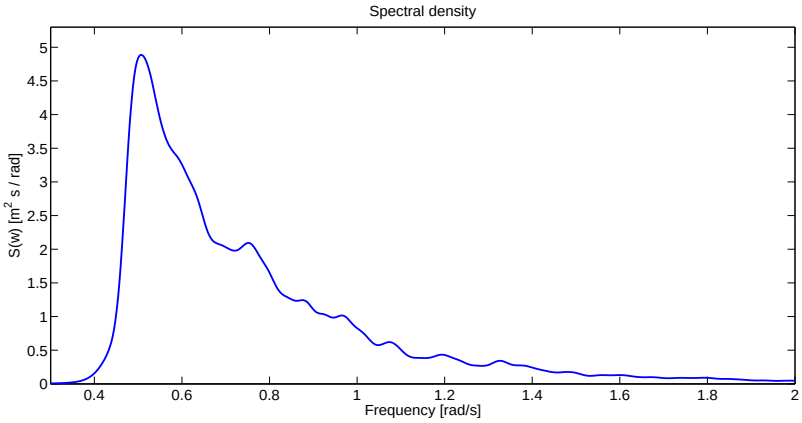


Figure 7: The wave spectrum corresponding to the measured specific three-hour wave record (3# gauge).

Finally, our numerical algorithm based on the Fast Fourier Transform technique and our proposed Transformed Rayleigh procedure are applied to calculate the wave crest height exceedance probabilities of the sea state with the surface elevation data measured at the Poseidon platform in the Japan Sea. The surface elevation data at the Poseidon platform were measured with three ultrasonic wave gauges located at the sea floor from 8:12 a. m. on Nov. 24, 1987 to 7:57 a. m. on Nov. 25, 1987 and three sets of data each consisting of 85547 wave elevation points had been obtained during the measurement. The water depth at the Poseidon platform is 41 m. Because a sea state remains *stationary* only within a short time period of less than three hours, we should divide each of the above three sets of data into eight short records respectively when we calculate the wave crest height distributions. In this study we have chosen a three-hour record of wave elevation points time series measured with the 3# ultrasonic wave gauge (Data source is from http://code.google.com/p/wafo/downloads/detail?name=wafo25.7z [32]. Please note that these data are used for academic research only and not for commercial purposes). In Fig. 7 the power spectrum corresponding to this specific three-hour wave record is shown.

Fig. 8 shows our calculated wave crest height exceedance probabilities for this measured specific three-hour sea state. The solid blue line in Fig. 8 represents the results of the wave crest height exceedance probabilities directly obtained from the measured three-hour wave elevation points at the Poseidon platform. The solid green line in Fig. 8 represents the Fast Fourier Transform nonlinear computation results of the wave crest height exceedance probability of this specific sea state based on 3500000 simulated wave elevation points. We can notice that the Fast Fourier Transform nonlinear computation results fit the measured data well.

In Fig. 8, the solid black dots represent the results of the wave crest height exceedance probabilities obtained from utilizing our proposed Transformed Rayleigh procedure. In applying the Transformed Rayleigh procedure, two 1025×1025 matrices $[Q+R]$ and $[Q-$

https://doi.org/10.4208/cicp.191214.071215a Published online by Cambridge University Press

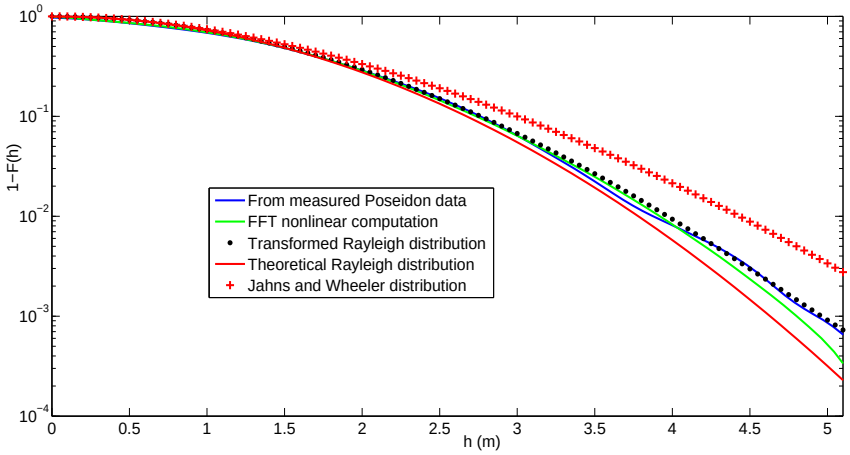


Figure 8: Wave crest height exceedance probabilities for a sea state with measured (3# gauge) data at the Poseidon platform.

R] as specified in Eq. (A.14) are first calculated and the elements in these two matrices are directly related to the wave spectrum as shown in Fig. 7 and the quadratic transfer functions r_{mn} and q_{mn}. We can see that the results from the Transformed Rayleigh procedure fit the measured data even slightly better than the Fast Fourier Transform nonlinear computation results. The reason for this is that the FFT simulated "uniformly" random waves do not always include all of the natural variability of the real sea waves. On the contrary, the transformed Rayleigh procedure focuses more on analytically following the intrinsic non-Gaussian nature of the real sea waves.

In Fig. 8, the small red "+" represents a wave crest height exceedance probability predicted by using the Jahns and Wheeler model (i.e. by using Eq. (5.2)) in which the value of Hs is taken to be four times the standard deviation of the surface elevation based on the spectrum in Fig. 7. We can find that the Jahns and Wheeler model gives poorer predictions in the wave crest height region of about [2m, 5.1m] than the Transformed Rayleigh distribution does. In Fig. 8, the solid red line represents the wave crest height exceedance probabilities calculated by using a Theoretical Rayleigh model. We can find that the Theoretical Rayleigh method underestimates the exceedance probabilities in the wave crest height region of about [2m, 5.1m].

Finally, it is mentioned that in this case, the time series computation with 3500000 wave elevation points and the post statistical processing for getting the green curve in Fig. 8 take about 168 seconds on a desktop computer (HP dx2310MT (VP784PA), Pentium (R) Dual-Core CPU E5300 @2.60GHz). By comparison, it takes less than 6 seconds to obtain the results of the wave crest height exceedance probabilities represented by the black solid dots in Fig. 8 by applying our Transformed Rayleigh procedure. The accuracy and efficiency of the Transformed Rayleigh procedure for calculating the wave crest height distributions of irregular Stokes waves are thus once again validated.

https://doi.org/10.4208/cicp.191214.071215a Published online by Cambridge University Press

6 Conclusions

The detailed mathematical formulas for a numerical algorithm based on the FFT technique and a proposed Transformed Rayleigh procedure for calculating the nonlinear crest distributions of irregular Stokes waves have been elucidated in this paper, and the corresponding computer codes have also been developed. The numerical algorithm based on the FFT technique and the proposed Transformed Rayleigh procedure have been applied for calculating the wave crest exceedance probabilities of a sea state with a Bretschneider spectrum corresponding to a water depth of 19.5m and a sea state with the surface elevation data measured at the Poseidon platform. It is demonstrated in these two cases that the numerical algorithm based on the FFT technique and the proposed Transformed Rayleigh procedure can offer better predictions than those from using the empirical wave crest distribution models. Meanwhile, it is found that our proposed Transformed Rayleigh procedure can compute nonlinear crest distributions more than 25 times faster than the numerical algorithm based on the FFT technique.

Acknowledgments

This research work is supported by the funding of an independent research project from the Chinese State Key Laboratory of Ocean Engineering (Grant No. GKZD010038).

Appendix A

We rewrite Eq. (3.1) as follows:

$$\begin{aligned}\eta_G(t) &= \mathrm{Re}\sum_{n=1}^{N} c_n e^{i(\omega_n t+\varepsilon_n)} = \sum_{n=1}^{N} c_n \cos(\omega_n t+\varepsilon_n)\\ &= \sum_{n=1}^{N} (a_n \cos(\omega_n t)+b_n \sin(\omega_n t)).\end{aligned} \tag{A.1}$$

In the above equation, $\omega_n = 2\pi n/T$, T is the time interval, c_n's are mutually independent of one another, and a_n and b_n are Gaussian random variables. Meanwhile, the coefficients of the above formula have the following properties [25]:

$$E\left[{a^2}_n\right] = E\left[{b^2}_n\right] = S_{\eta\eta}(\omega)\,d\omega, \qquad E[a_n b_m] = 0, \tag{A.2}$$

$$E[a_m a_n] = E[b_m b_n] = 0 \qquad m \neq n, \tag{A.3}$$

$${c^2}_m = {a^2}_m + {b^2}_m, \tag{A.4}$$

$$\varepsilon_m = \tan^{-1}(-b_m/a_m). \tag{A.5}$$

In Eq. (A.2) and Eq. (A.3), the operator E denotes mathematical expectation. In Eq. (A.2) $S_{\eta\eta}(\omega)$ is the one-sided wave spectrum (i.e., wave power spectral density function) and

https://doi.org/10.4208/cicp.191214.071215a Published online by Cambridge University Press

$d\omega = 2\pi/T$. The spectrum of the process $\eta_G(t)$ given by Eq. (A.1) tends to the exact spectrum $S_{\eta\eta}(\omega)$ as N, $T \to \infty$. For the present statistical analysis it is more helpful to re-express the complex term appearing in Eq. (A.1) in the form [25]:

$$c_m e^{i(\omega_m t+\varepsilon_m)} = \sqrt{S_{\eta\eta}(\omega_m)d\omega}(x_m + iy_m). \tag{A.6}$$

With comparison with Eq. (A.1) shows that:

$$x_m\sqrt{S_{\eta\eta}(\omega_m)d\omega} = a_m\cos(\omega_m t)+b_m\sin(\omega_m t), \tag{A.7}$$

$$y_m\sqrt{S_{\eta\eta}(\omega_m)d\omega} = a_m\sin(\omega_m t)+b_m\cos(\omega_m t). \tag{A.8}$$

The fact that a_m and b_m are Gaussian random variables implies that at any fixed time t, x_m and y_m will also be Gaussian random variables. Further, Eq. (A.2) and Eq. (A.3) imply that:

$$\begin{aligned} &E\left[x^2{}_m\right] = E\left[y^2{}_m\right] = 1, \qquad && E[x_m y_n] = 0, \\ &E[x_m x_n] = E[y_m y_n] = 0, && m \neq n. \end{aligned} \tag{A.9}$$

In this study we consider $\eta^{(2)}$ in Eq. (2.10) at a specific reference location (say $x = 0$) and rewrite it as $\eta_{SO}(t)$ to indicate that it is the second order correction part of the waves. For a total time period T of computation, Eq. (2.10) can be written as:

$$\eta_{SO}(t) = \mathrm{Re}\sum_{m=1}^{N}\sum_{n=1}^{N} c_m c_n\left[r_{mn}e^{i(\omega_m t+\varepsilon_m+\omega_n t+\varepsilon_n)}+q_{mn}e^{i(\omega_m t+\varepsilon_m-\omega_n t-\varepsilon_n)}\right]. \tag{A.10}$$

Finally, the entire irregular Stokes waves $\eta(t)$ can be obtained by combing the linear part $\eta_G(t)$ and the second order part $\eta_{SO}(t)$, i.e.:

$$\eta(t) = \mathrm{Re}\sum_{m=1}^{N} c_m e^{i\phi_m}+\mathrm{Re}\sum_{m=1}^{N}\sum_{n=1}^{N} c_m c_n\left[r_{mn}e^{i(\phi_m+\phi_n)}+q_{mn}e^{i(\phi_m-\phi_n)}\right] \tag{A.11}$$

where

$$\phi_m = \omega_m t+\varepsilon_m, \qquad \phi_n = \omega_n t+\varepsilon_n. \tag{A.12}$$

The terms r_{mn} and q_{mn} are the same as shown in Eqs. (2.12)-(2.13). It can be seen that $r_{mn} = r_{nm}$; $q_{mn} = q_{nm}$. Using Eq. (A.6), Eq. (A.11) can be rewritten as:

$$\begin{aligned} \eta(t) = &\mathrm{Re}\sum_{m=1}^{N}\sqrt{S_{\eta\eta}(\omega_m)d\omega}(x_n+iy_n) \\ &+\mathrm{Re}\sum_{m=1}^{N}\sum_{n=1}^{N}[s_n s_m r_{mn}(x_n+iy_n)(x_m+iy_m)+s_n s_m q_{mn}(x_n+iy_n)(x_m-iy_m)]. \end{aligned} \tag{A.13}$$

https://doi.org/10.4208/cicp.191214.071215a Published online by Cambridge University Press

Collecting real parts, Eq. (A.13) can be re-written in the following matrix notation [25]:

$$\eta(t)=\mathbf{s}^T\mathbf{x}+\mathbf{x}^T[Q+R]\mathbf{x}+\mathbf{y}^T[Q-R]\mathbf{y} \tag{A.14}$$

where Q and R are real symmetric matrix whose nmth components are $s_n s_m q_{mn}$ and $s_n s_m r_{mn}$ respectively, $\mathbf{s}$, $\mathbf{x}$ and $\mathbf{y}$ are vectors whose nth components are s_n, x_n and y_n respectively and $s_n=\sqrt{S_{\eta\eta}(\omega_m)d\omega}$. By performing an eigenvalue decomposition, the above equation becomes [25]:

$$\eta(t)=\mathbf{s}^T\mathbf{x}+\mathbf{x}^T{P_1}^T\Lambda_1 P\mathbf{x}+\mathbf{y}^T{P_2}^T\Lambda_2 P_2\mathbf{y} \tag{A.15}$$

where Λ_i is a diagonal matrix with the eigenvalues in the respective diagonal and P_i contains the corresponding eigenvectors per row. Introducing a new set of Gaussian random variables Z_j, such that:

$$\mathbf{Z}=\begin{bmatrix} P_1 & 0 \\ 0 & P_2 \end{bmatrix}\begin{bmatrix} \mathbf{x} \\ \mathbf{y} \end{bmatrix} \tag{A.16}$$

we can write the stochastic process $\eta(t)$ as (this is called the Kac-Siegert solution):

$$\eta(t)=\sum_{j=1}^{2N}\beta_j Z_j+\lambda_j {Z_j}^2 \tag{A.17}$$

where Z_j are independent Gaussian processes with unit variance, and β_j and λ_j are coefficients computed based on the information provided by the sea spectrum $S_{\eta\eta}(\omega)$, which is chosen for a given sea state. Specifically, the coefficients in the above equation are computed as follows:

$$\boldsymbol{\beta}=\begin{bmatrix} P_1\mathbf{s} \\ 0 \end{bmatrix} \qquad \boldsymbol{\lambda}=\begin{bmatrix} (\Lambda_1)^d \\ (\Lambda_2)^d \end{bmatrix} \tag{A.18}$$

where $(\Lambda_i)^d$ denotes a column vector formed by the diagonal elements of Λ_i.

Appendix B

In applying the Transformed Rayleigh procedure, the transformation model is chosen to be a monotonic exponential function, calibrated such that the first three moments of the transformed model $G(\tilde{\eta}(t))$ match the moments of the true process $\eta(t)$. Information about the moments of the process can be obtained by resorting to theoretical models. Here we should note that the mean of a process is equal to its first moment. The standard deviation of a process is equal to the square root of its second central moment. The third central moment of a process is directly related to the skewness of the process, and the fourth central moment of a process is directly related to the kurtosis of the process.

https://doi.org/10.4208/cicp.191214.071215a Published online by Cambridge University Press

We show below the procedures for obtaining the mean, standard deviation, skewness and kurtosis of a process.

We recall Eq. (4.1) for the surface elevation $\eta(t)$ in the main body of the text:

$$\eta(t)=\sum_{j=1}^{2N}\beta_j Z_j+\lambda_j {Z_j}^2 \tag{B.1}$$

where Z_j are independent Gaussian processes with unit variance, and β_j and λ_j are coefficients computed based on the information provided by the sea spectrum $S_{\eta\eta}(\omega)$, which is chosen for a given sea state. We define an individual component of the above equation as:

$$U_j=\beta_j Z_j+\lambda_j {Z_j}^2. \tag{B.2}$$

The characteristic function $M_j(\theta)$ of U_j is obtained as:

$$M_j(\theta)=E\left[e^{i\theta U_j}\right]=\int_{-\infty}^{\infty} e^{i\theta\left(\beta_j Z_j+\lambda_j {Z_j}^2\right)}p\left(Z_j\right)dZ_j \tag{B.3}$$

where $p(Z_j)$ is the probability density function of Z_j, the fact that Z_j is Gaussian with unit variance implies that:

$$p\left(Z_j\right)=\frac{1}{\sqrt{2\pi}}\exp\left(-1/2{Z_j}^2\right). \tag{B.4}$$

Therefore, Eq. (B.3) can be evaluated to obtain [25]:

$$M_j(\theta)=\frac{1}{\sqrt{1-2i\lambda_j\theta}}\exp\left[-\frac{{\beta_j}^2\theta^2}{2\left(1-2i\lambda_j\theta\right)}\right] \tag{B.5}$$

where the standard result $\int_{-\infty}^{\infty}\exp(-(1/2)(Z/a)^2)dZ=\sqrt{2\pi}a$ has been utilized. Utilizing the fact the variables U_j are statistically independent, the characteristic function of $\eta(t)$, $M(\theta)$, can be obtained as:

$$M(\theta)=E\left[e^{i\theta\eta}\right]=\prod_{j=1}^{2N}M_j(\theta). \tag{B.6}$$

Because the characteristic function and the probability density form a Fourier transform pair, an expression for the probability density function can now be obtained as:

$$p(\eta)=\frac{1}{2\pi}\int_{-\infty}^{\infty}\exp(-i\eta\theta)M(\theta)d\theta. \tag{B.7}$$

The nth cumulant of a random process is defined in terms of the characteristic function $M(\theta)$ as follows [25]:

$$k_n=\frac{1}{i^n}\frac{d^n}{d\theta^n}\ln[M(\theta)]|_{\theta=0}. \tag{B.8}$$

https://doi.org/10.4208/cicp.191214.071215a Published online by Cambridge University Press

k_1 can be shown to be the mean value μ of the process, while k_2 can be shown to be the variance (square of the standard deviation σ^2) of the process. The coefficients k_3 and k_4 are often used as a measure of the extent to which a random process is non-Gaussian, with k_3/σ^3 being referred to as the skewness and k_4/σ^4 being referred to as the kurtosis. In the present case the cumulant can be obtained by substituting Eqs. (B.3) and (B.5) in Eq. (B.8), to give [25]:

$$k_n=\sum_{j=1}^{2N}\frac{1}{2}(2\lambda_j)^n\left[(n-1)!+\left(\frac{\beta_j}{2\lambda_j}\right)^2 n!\delta_{n1}\right] \tag{B.9}$$

where δ_{n1} is equal to zero for $n=1$ and is equal to unity otherwise. Specifically, the first four cumulants are obtained as follows [25]:

$$\begin{aligned} k_1&=\sum_{j=1}^{2N}\lambda_j, & k_2&=\sum_{j=1}^{2N}{\beta_j}^2+2\sum_{j=1}^{2N}{\lambda_j}^2,\\ k_3&=6\sum_{j=1}^{2N}\lambda_j{\beta_j}^2+8\sum_{j=1}^{2N}{\lambda_j}^3, & k_4&=48\sum_{j=1}^{2N}{\lambda_j}^2{\beta_j}^2+48\sum_{j=1}^{2N}{\lambda_j}^4, \end{aligned} \tag{B.10}$$

where β_j and λ_j are coefficients computed by utilizing Eq. (A.18) in the Appendix A.

References

[1] S.K. Chakrabarti, Handbook of Offshore Engineering, Elsevier Science, (2005): 197-277.
[2] K. Al-Salem, W. Al-Nassar, A. Tayfun, Risk analysis for capsizing of small vessels, Ocean Eng., 33 (2006): 788-797.
[3] M.S. Longuet-Higgins, On the statistical distribution of the heights of sea waves, J. Mar. Res., 11 (1952): 245-266.
[4] S.K. Chakrabarti, Hydrodynamics of Offshore Structures. Computational Mechanics Publications Inc., 1987.
[5] M.K. Ochi, Ocean Waves, The Stochastic Approach, Cambridge University Press, (1998): 2-4.
[6] M. Onorato, A.R. Osborne, M. Serio, Observation of strongly non-Gaussian statistics for random sea surface gravity waves in wave flume experiments, Phys. Rev. E, 70 (2004): 067302, 1-4.
[7] F. Fedele, On wave groups in a Gaussian sea, Ocean Eng., 33 (2006): 2225-2239.
[8] P.A.E.M. Janssen, Nonlinear four-wave interactions and freak waves, J. Phys. Oceanogr., 33 (2003): 863-884.
[9] A.I. Dyachenko, and V.E. Zakharov, Modulation instability of stokes wave freak wave, JETP Letters, 81(6) (2005): 255-259.
[10] V.E. Zakharov and R.V. Shamin, Probability of the occurrence of freak waves, JETP Letters, 91(2) (2010): 62-65.
[11] G.Z. Forristall, Wave crest distributions: Observations and second-order theory, J. Phys. Oceanogr., 30:8 (2000): 1931-1943.
[12] M.A. Tayfun, Narrow-band nonlinear sea waves, J. Geophys. Res., 85 (1980): 1548-1552.
[13] V.P. Lukomsky, I.S. Gandzha, D.V. Lukomsky, Computational analysis of the almost-highest waves on deep water, Comput. Phys. Commun., 147(1-2) (2002): 548-551.

https://doi.org/10.4208/cicp.191214.071215a Published online by Cambridge University Press

[14] V.P. Lukomsky, I.S. Gandzha, D.V. Lukomsky, Steep sharp-crested gravity waves on deep water, Phys. Rev. Lett., 89(16) (2002): 164502.
[15] V.P. Lukomsky, I.S. Gandzha, Fractional Fourier approximations for potential gravity waves on deep water, Nonlinear Processes in Geophysics, 109(6) (2003): 599-614.
[16] Y.G Wang, and Y.Q. Xia, Simulating mixed sea state waves for marine design. Appl. Ocean Res., 37 (2012): 33-44.
[17] C. Viotti, D. Dutykh, J. Dudley, F. Dias, The emergence of coherent wave groups in deep-water random sea, Phys. Rev. E, 87(6), 063001 (2013):1-10.
[18] A. Toffoli, E. Bitner-Gregersen, M. Onorato, A.V. Babanin, Wave crest and trough distributions in a broad-banded directional wave field, Ocean Eng., 35 (2008): 1784-1792.
[19] J.W. Cooley, J.W. Tukey, An algorithm for the machine calculation of complex Fourier series, Math. Comput., 19:90 (1965): 297-301.
[20] H.M. Yan, Y.M. Liu, An efficient high-order boundary element method for nonlinear wave-wave and wave-body interactions, J. Comput. Phys., 230 (2011): 402-424.
[21] http://www.mathworks.cn/cn/help/matlab/ref/fft.html.
[22] J.N. Sharma, R.G. Dean, Second order directional seas and associated wave forces, Soc. Petroleum Engineers J., 4, (1981): 129-140.
[23] S.F. Smith, M.J.R. Hoyle, R.V. Ahilan, R.J. Hunt, M.R. Marcom, 3D nonlinear wave spreading on jackup loading and response and its impact on current assessment practice, Offshore Technology Conference, (2006): OTC 18266, 1-13.
[24] T. Marthinsen, On the Statistics of Irregular Second-Order Waves, Stanford Report RMS-11, 1992.
[25] R.S. Langley, A statistical analysis of non-linear random waves, Ocean Eng., 14(5) (1987): 389-407.
[26] K. Hasselmann, On the non-linear energy transfer in a gravity-wave spectrum Part I. General theory. J. Fluid Mech., 12 (1962): 481-500.
[27] V.P. Krasitskii, Canonical transformation in a theory of weakly nonlinear waves with a non-decay dispersion law, Sov. Phys. JETP, 71(5) (1990): 921-927.
[28] M. Shinozuka, G. Deodatis, Simulation of stochastic processes by spectral representation, Appl. Mech. Rev. ASME, 44:4 (1991): 191-204.
[29] M.K. Ochi, Probability distribution applicable to non-Gaussian random processes, Probabilist. Eng. Mech., 9 (1994): 255-264.
[30] Y.G. Wang, and Y.Q. Xia, Calculating nonlinear wave crest exceedance probabilities using a Transformed Rayleigh method, Coast. Eng., 78 (2013): 1-12.
[31] Y. Kiyokazu, O. Yutaka, S. Masakatsu, S. Kinji, At sea experiment of a floating offshore structure, Part 5, Measurement of stress range distributions for fatigue analysis, J. Soc. Naval Architects Japan, 170, (1991): 609-618. (In Japanese).
[32] http://code.google.com/p/wafo/downloads/detail?name=wafo25.7z.

https://doi.org/10.4208/cicp.191214.071215a Published online by Cambridge University Press